Real-World Subsynchronous Oscillation Events in Power Grids with High Penetrations of Inverter-Based Resources

Yunzhi Cheng, *Senior Member, IEEE*, Lingling Fan, *Fellow, IEEE*, Jonathan Rose, *Senior Member, IEEE*, Shun-Hsien Huang, *Senior Member, IEEE*, John Schmall, *Senior Member, IEEE*, Xiaoyu Wang, *Senior Member, IEEE*, Xiaorong Xie, *Senior Member, IEEE*, Jan Shair, *Member, IEEE*, Jayanth Ramamurthy, *Senior Member, IEEE*, Nilesh Modi, *Senior Member, IEEE*, Chun Li, *Senior Member, IEEE*, Chen Wang, *Member, IEEE*, Shahil Shah, *Senior Member, IEEE*, Bikash Pal, *Fellow, IEEE*, Zhixin Miao, *Senior Member, IEEE*, Andrew Isaacs, *Senior Member, IEEE*, Jean Mahseredjian, *Fellow, IEEE*, Jenny Zhou *Senior Member, IEEE*

IEEE PES IBR SSO Task Force

Abstract—This paper presents a survey of real-world subsynchronous oscillation events associated with inverter-based resources (IBR) over the past decade. The focus is on those oscillations in the subsynchronous frequency range known to be influenced by power grid characteristics, e.g., series compensation or low system strength. A brief overview of the historical events is presented followed by detailed descriptions of a series of events. This paper also examines causation mechanisms and proposes future research directions to meet grid needs worldwide.

Index Terms—Inverter-based resources; oscillations; stability.

I. INTRODUCTION

PENETRATIONS of inverter-based resources (IBRs) are increasing worldwide. The maximum instantaneous penetration levels of IBRs in South Australia, Texas, Ireland, and Tasmania have reached 150%, 66%, 92%, and 95%, respectively [1]. The operation with such high levels of IBRs has introduced undesirable dynamics, including subcycle overvoltage [2], ac overcurrents [3] and subsynchronous oscillations (SSOs) [4], [5]. Stability issues related to IBRs have caught attention by the IEEE Power & Energy Society. In view of

this, stability definition and classification were revisited and extended to include converter-driven stability issues in [6]. Understanding these dynamics has led to the development of sophisticated solutions such as SSO damping controllers for type-3 wind turbines [5]. On the other hand, many oscillatory phenomena remain to be understood and mitigated, such as oscillations caused by low system strength or weak grid [7]. According to a 2020 system strength workshop held by Australian Energy Market Operator (AEMO) [8], weak grid associated stability challenges are viewed as the most significant challenges to higher IBR penetrations.

SSOs are not uniquely related to IBRs. In the past, SSOs have been observed in synchronous generators, HVdc systems and flexible ac transmission systems (FACTS). Lessons learned from the past can help us relate and solve today's stability issues facing IBR integration. In 1971, Mohave power plant in Nevada suffered mechanical shaft damage due to the interaction of an electric resonance mode related to series compensation and the torsional modes of the steam turbine generator [9]. In 1977, the first SSO in HVdc was observed at Square Butte in North Dakota. The current control loop of an HVdc converter near a generating plant interacted with a 11.5-Hz torsional mode and drove the torsional mode unstable upon switching out one ac line [10]. It is found that the the conventional line commuted control-based HVDC's current and power control can provide negative electrical damping in 10-30 Hz range. This SSO can be easily mitigated through proper design of HVDC control. Furthermore, for voltage source converter (VSC)-HVDC, SSOs have also been observed in real world operation and simulation studies when the ac grid strength becomes weak. In [11], SSOs are identified to be influenced by short-circuit ratio (SCR) and phase-locked-loop (PLL) parameters. Moreover, for static var compensators (SVCs) installed in weak grid, SSOs can also appear [12].

IBR controls have a wide timescale, thus IBR oscillations are not limited to the subsynchronous range. According to the review conducted in [6], hundred Hz and kilo Hz dynamics are possible. Oscillations above synchronous frequency at hundred

Hz have been observed in real world. For example, in Europe, oscillations in the frequency range of a few hundred Hz to 800 Hz have been observed in offshore wind power plants (WPP) [13], [14] due to the interaction of WPP and the collector cable.

The focus of the current paper is to provide a survey of real-world subsynchronous oscillation events associated with WPPs and solar PVs. A brief historical overview is first presented, followed by the detailed descriptions of actual events in Section II and Section III. The events are roughly categorized as SSO associated with type-3 WPPs interconnected with series compensated networks (in short, series capacitor SSO) and SSO associated with various IBRs (e.g., type-3 WPPs, type-4 WPPs, and solar PVs) with weak grid interconnection (in short, weak grid SSO). Section II presents oscillation events associated with series compensation and wind farms. Mechanism analysis of series capacitor SSO is also reviewed in this Section. Section III presents weak grid oscillation events. This section builds off the work of the IEEE PES TR-80 wind SSO task force report [5] to cover greater detail and include recent oscillation events in eastern U.S., Canada, and Australia. Section IV presents a brief literature review to summarize what are the possible mechanisms of weak grid SSO. Section V compares the literature and various real-world events, and raises five relevant questions for deep think. Section VI concludes by examining the challenges and suggesting future research directions.

A. Timeline of the events

The timeline of the nineteen events is as follows.

1) (2007) An SSO event occurred in south central Minnesota when a 100-MW type-3 WPP was inadvertently left radially connected to a 345-kV series-compensated transmission line. Digital fault records (DFR) revealed a 9.44-Hz current oscillation frequency [5], [15].

2) (2009) Tripping of a transmission line left multiple type-3 WPPs radially connected to a series compensated 345-kV transmission line in South Texas. Large 20-30 Hz overcurrents appeared within 150 ms, causing severe damage to the series capacitor and WPPs [5], [16], [17].

3) (2010) Oklahoma Gas & Electric (OG&E) observed 13-Hz oscillations at two nearby WPPs [4]. The oscillations occurred when wind farm output was above 80 percent of its rated level and the magnitude of oscillation reached 5% of the 138-kV voltage. OG&E curtailed the plant's output until the manufacturer made modifications to the wind power conversion system.

4) (2011) 4-Hz oscillations were observed at a type-4 WPP in Texas region after a transmission line tripped [18].

5) (2011-2014) Since 2011, oscillations were observed by BPA during high wind generation conditions [4]. A 450-MW type-4 WPP located in Oregon was identified as the source. In summer 2013, BPA's phasor measurement unit (PMU) monitoring system identified 5-Hz oscillations in voltage, real and reactive power. In early 2014, BPA detected 14-Hz oscillations. Reactive power oscillations reached 80 Mvar peak to peak while power reached

85% of the rated level. The wind generator manufacturer upgraded their voltage control and no oscillations have been detected since.

6) (2011-2012) OG&E reported two wind oscillation events, one in December 2011 and another one in December 2012. Both were triggered due to line outage. For the 2012 event, 3-Hz oscillations appeared at a 60-MW WPP after a line outage [4]. Curtailing the power helped restore the system. OG&E worked with the WPP manufacturer to tune the WPP control parameters, resolving the issue.

7) (2012-2013) During the one-year period, more than 58 oscillation events were reported in North China with oscillation frequency of 6-9 Hz. The oscillations occurred due to interaction between type-3 WPPs and 500-kV double circuit series compensated transmission lines connecting Guyuan station with Inner Mongolia and North China grids [5], [19].

8) (2014-2015) 30-Hz oscillations appeared when type-4 WPPs located in Xinjiang China with connection to a 750-kV system started to export power. The oscillations spread to the main grid and caused the subsynchronous resonance (SSR) protection relay of a 600-MW thermal power plant located 48 km away to trip the power plant. Initial research indicated that such oscillations are triggered due to interaction between WPPs with weak grid interconnection [20].

9) (2015) Poorly damped 20-Hz oscillations were observed in root mean square (RMS) voltage of a 44-kV distribution feeder in Hydro One, Canada after the energizing of a 30-Mvar shunt capacitor at the substation [21]. This feeder has three 10-MVA solar farms connected. Fast Fourier transform (FFT) analysis showed 80 Hz in instantaneous currents.

10) (2016) In November 2016, PMUs captured oscillations for multiple days at a solar farm in AEP footprint [4].

11) (2017) 37-Hz and 63-Hz oscillations were observed in instantaneous voltages and currents at a 600-MW type-3 WPP (300 turbines, each 2 MW) connected to a 220-kV grid in northwest China [22] and [23]. The 63-Hz oscillations dominate phase voltages. Both resonances are of positive sequence. The oscillations have been resolved by grid strengthening (an additional 500 kV line was constructed and put into service) and WPP converter control update.

12) (2017) 7-Hz oscillations in real power, reactive power, and RMS voltage appeared in a First Solar's solar farm in California [24].

13) (2017) Three separate SSO events occurred in South Texas [5]. The frequency range is 22-26 Hz in instantaneous currents. WPP vendors fixed the issue by updating WPP converter control software.

14) (2015-2019) 7-Hz voltage oscillations were observed in Australia's West Murray zone under low system strength and high penetrations of IBRs [25], [26].

15) (2018-2019) 3.5-Hz oscillations were observed in real power and reactive power measurement for two 230-kV type-4 WPPs in Hydro One after a planned 230-kV bus

outage [27]. The outage caused a significant reduction in system strength viewed from the WPPs. A nearby 150-kV solar PV also reported undamped reactive power oscillations.

16) (2019): 9-Hz oscillations were observed 10 minutes before the August 2019 Great Britain (GB) power system disruption [28]. Weak grid oscillations were later identified as the reason why an 800-MW offshore WPP went to the de-loading stage. The WPP vendor upgraded the control software afterwards.

17) (2020) 17-19 Hz voltage oscillations were reported for the West Murray zone in Australia [8].

18) (2021) 22-Hz oscillations in RMS voltage related to a solar PV farm were reported by Dominion Energy in eastern U.S. [29]. In instantaneous currents and voltages, 38-Hz and 82-Hz components were observed.

19) (2021) 8-Hz oscillations in RMS voltage were observed in Scotland on August 24 2021 [30]. The disturbances lasted 20-25 seconds on two occasions, approximately 30 minutes apart. The oscillations were mitigated after some traditional plants were put back to the system. The Scottish system has a very high penetration of wind farms. The root cause of the oscillation is currently under investigation.

II. SERIES CAPACITOR SSO

Events #1, #2, #7, #13 are all associated with type-3 WPPs at radial connection with series capacitors and they are termed *series capacitor SSO*.

A. Minnesota event in 2007: 9.44-Hz SSO

In 2007, an overcurrent SSO event was reported in south central Minnesota. Within a span of about 0.3 seconds, the phase current magnitude increased from less than 100 A to around 1000 A.

As wind power-based generation rapidly increased in southern Minnesota from 2004 to 2007, significant transmission system improvements were required. One such improvement involved installing 60% series compensation on a 54-mile 345-kV transmission line to improve transfer capability. Fig. 1 shows the one-line diagram including the ring-bus where the WPP was interconnected.

As part of the planning work for installing the series capacitors, a traditional SSR screening analysis was performed to examine interaction with nearby existing combustion turbine generators. This analysis identified low SSR risk and no SSR relays were installed. It was assumed at that time that the nearby wind turbines, based on type-3 technology, were not susceptible to SSR. On October 8, 2007, breakers Brk5 and Brk6 were opened as part of a regular system switching procedure, placing the WPP and the combustion turbine generator units in a radial connection with the series capacitor. The result was undamped current oscillations. Local DFR data are shown in Fig. 2. Some wind turbine components were damaged during this event along with damage to nearby buswork. Post-event analysis indicated the oscillation mode was not coincident with the combustion turbine generator torsional modes.
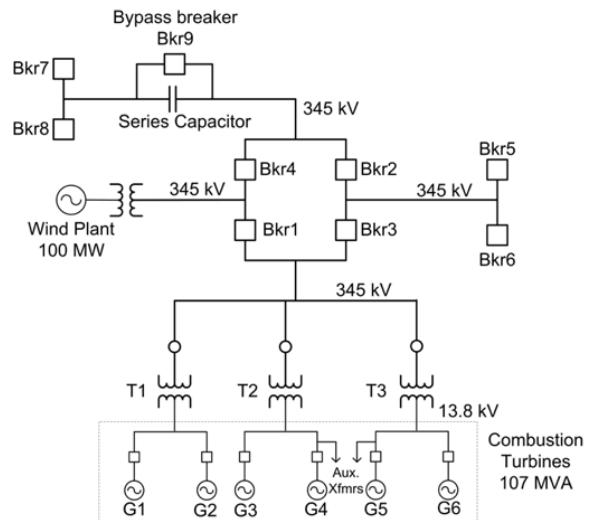
Fig. 1: One-line diagram of the 345-kV system with series compensation in south central Minnesota. Source: J. Ramamurthy; used with permission.
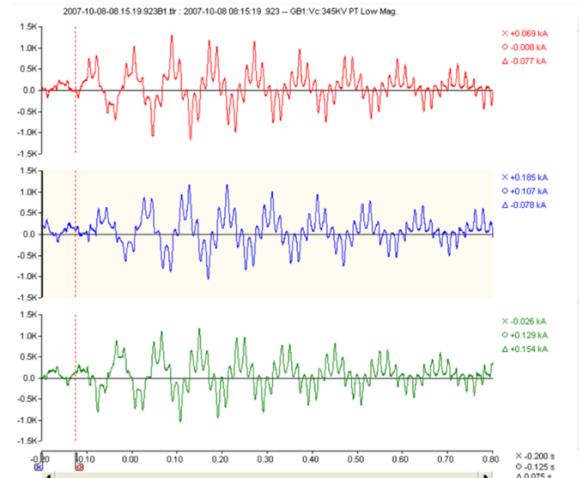
Fig. 2: Minnesota 2007 event. DFR records of phase current measurement. Source: J. Ramamurthy; used with permission.

B. Texas events in 2009, 2017: 20-30 Hz SSO

(2009) As shown in Fig. 3, a cluster of type-3 WPPs totaling 680 MW was connected to the 345-kV Ajo station. The series compensation at Rio Hondo had two stages: 33% and 17% (total 50% compensation) based on the total reactance of the transmission line between Rio Hondo and Lon Hill. In 2009, a fault tripped the Ajo – Lon Hill line. Rapid subsynchronous current oscillations in the range of 20 to 30 Hz appeared almost immediately within 150 ms, causing high voltages and resulting in damage to both the series capacitors and to the wind turbine crowbar circuits. DFR records are shown in Fig. 4.

It is worth noting that because the Ajo station taps a long series-compensated line, an outage on the north segment leaves the WPPs experiencing an 80% effective compensation level. After repairs were made, an SSR relay was installed as a temporary solution to trip the transmission spur feeding the WPPs. When the Rio Hondo to Lon Hill transmission line was later reconductored for a higher current rating, the
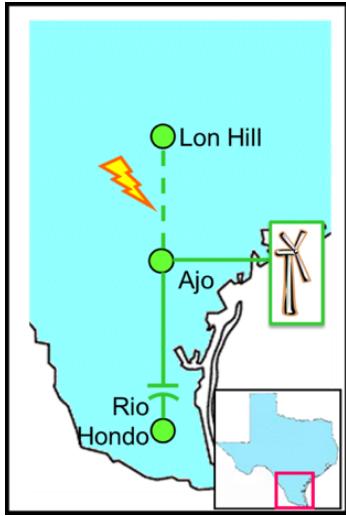
Fig. 3: A series compensated line in South Texas. Source: ERCOT; used with permission.

compensation level was permanently reduced to 30%, thereby reducing risk. The WPPs also later confirmed installation of subsynchronous damping controllers and the relay was considered no longer considered unecessary and retired.
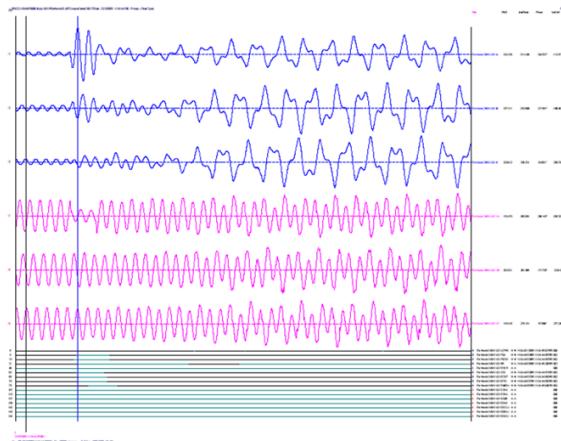

Fig. 4: Texas 2009 event. Measurement data captured by Rio Hondo SEL421 at Ajo. Row 1-3: phase current. Row 4-6: phase voltage. 24-Hz oscillations appear in the phase currents. Source: ERCOT; used with permission.

(2017) ERCOT experienced three SSO events in 2017, all related to the series compensation on the Lobo – N Edinburg 345kV line.

This event was significant because all wind farms had been previously studied for SSO and damping controllers were installed. Inaccuracies in the PSCAD models was partly to blame.

Several WPPs connect into this long transmission line which connects the Lower Rio Grande Valley to Laredo; all utilized type-3 turbines. Because of their interconnection locations, it is possible to form a radial connection between the WPPs and the series capacitors by opening either end of the line and the three events in 2017 all involved such contingencies. Following each event, 20 to 30 Hz oscillations were lasting until the WPPs tripped off or the series capacitors automatically bypassed. No
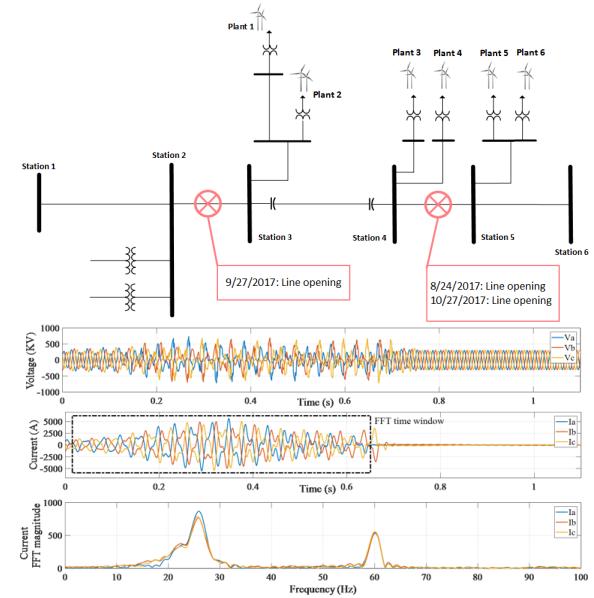
Fig. 5: Texas 2017 event: the system topology and measurement records. Source: ERCOT; used with permission.

damage was reported. The system topology and DFR records are shown in Fig. 5.

It took one year to replicate the problem in simulation and design an acceptable control solution. It is worth to note that the IBR task force members at University of South Florida set up a test bed to replicate the three 2017 events with public available data only in [31]. Interested readers may refer to [31] for the detailed information on the test bed.

C. North China 2012-2013: 6-9 Hz SSO

6-9 Hz SSO was observed in north China WPPs in 2012-2013. The location is more than 300 km away from a load center. The system topology is shown in Fig. 6. A network of 220-kV lines collects the power from each WPP, and a 500-kV double-circuit backbone transmission line exports the power to the Northern and Inner Mongolia grids. The two 500-kV circuits are series compensated at 40% and 45% levels, respectively. The equivalent series compensation level can be as low as 6.66% [19].
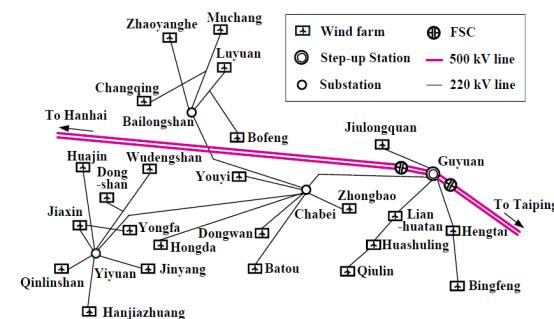

Fig. 6: North China 500-kV lines with series compensation [19]. WPPs are connected to the 500-kV lines. Source: X. Xie; used with permission.
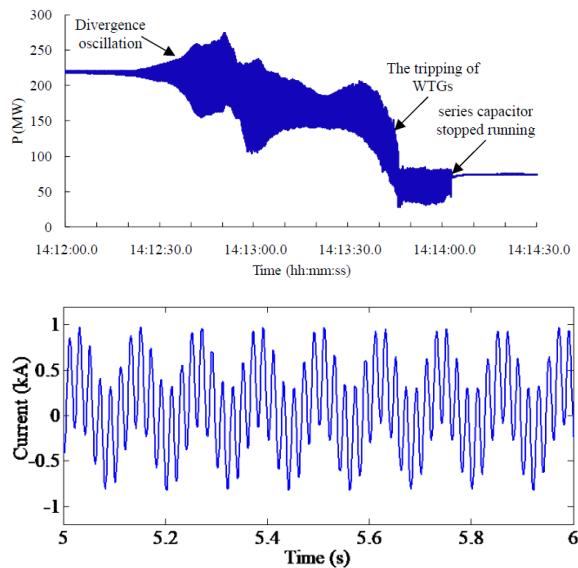
Fig. 7: (2012-2013) North China series capacitor SSO: power and phase current measurement. Oscillation frequency is 8.1 Hz in phase current [19]. Source: X. Xie; used with permission.

There are 24 WPPs of three types in the area with an installed capacity of 4224 MW. The percentages of type-2, type-3 and type-4 are 82.8%, 15.4% and 1.8%, respectively.

Since the installation of series capacitors in October 2010, SSO has occurred under the condition that all the series compensated capacitors of all the 500-kV lines are put into operation and the 220-kV wind power system is operating normally. With a large number of new WPPs placed into service since December 2012, the subsynchronous resonance is much more likely to happen. From December 2012 to December 2013, 58 SSO events in the wind power system were detected. A typical formation of one of the SSO events is presented in Fig. 7. The magnitude of oscillation grows until reaching a sustained level. The oscillation disappears if one of the four series compensations is taken out of service.

D. Mechanism Analysis of SSO in type-3 WPPs with series compensation interconnections

The common mechanism of SSO between series capacitors and type-3 wind generation is the induction generator effect (IGE). This mechanism is unlike the 1971 Mohave power plant SSR event for which torsional interactions were the cause. The reason is that the natural frequency of wind turbine shaft can be as low as 1.8 Hz. To have possible torsional interactions, the frequency of SSOs in the phase current should be about 48 Hz for a 50-Hz system or about 58 Hz for a 60-Hz system. All the type-3 wind farm SSOs have frequencies below 30 Hz in phase currents. Specifically, wind farm SSO events in North China (event #7) have 6-9 Hz in phase currents [19]. It is thus not possible for wind turbines subject to torsional interactions.

At the electric LC resonant frequency, a doubly-fed induction generator's slip is negative. Lower wind speed further reduces the negative equivalent resistance.

The mechanism can be explained using a steady-state induction machine circuit by replacing the slip by a Laplace transfer function [32]. Fig. 8 illustrates a type-3 wind turbine that is radially connected to a series compensated network. The slip can be represented by $slip = 1 - \frac{j\omega_m}{s}$, where ω_m is the per unit rotor speed. s is the Laplacian transform variable.

At the network resonance frequency range, $slip = 1 - \frac{j\omega_m}{j\omega_{LC}}$. Suppose that the machine speed is 0.75 p.u. and the LC resonance frequency is 0.70 p.u .due to a series compensation level of 50%. The resulting slip is $1 - 0.75/0.70 = -0.07$. The equivalent resistance becomes $-14r'$; thus, the system may be subject to instability.

In addition, as stated by E.V. Larsen [33], the rotor side converter's current control logic (dq-frame PI control) effectively increases the equivalent rotor-side resistance, which translates to a negative resistance viewed from stator; thus, the rotor side converter control may exacerbate SSOs. This finding is also presented in [34] where an impedance model of a type-3 wind farm with rotor side converter current control included is derived and used for stability analysis.
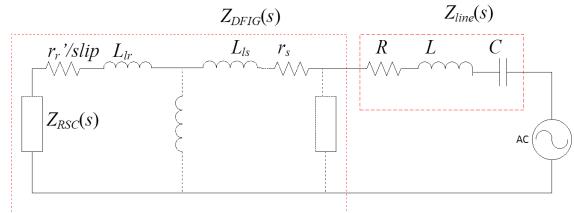

Fig. 8: Circuit diagram of a type-3 wind farm connected to an RLC circuit [32].

To maintain efficient energy capture, modern wind turbines are variable speed devices; they reduce rotor speed to match lower wind speeds. Comparing 0.95 p.u. versus 0.75 p.u. rotational speeds, it is obvious that both lead to negative resistance. However, the latter leads to a smaller absolute value of slip and a larger negative resistance, which explains a higher risk of SSO under low wind speed condition. For the same wind speed, a higher series compensation level leads to a higher LC resonance frequency. Suppose that the machine speed is nominal at 1 p.u.. Then a 50% compensation level leads to 0.7 p.u. LC resonance frequency and -0.4286 slip, while 75% compensation level leads to 0.866 p.u. LC resonance frequency and -0.1547 slip. Thus, the higher the compensation level, the smaller the absolute value of slip, and the worse the potential instability.

With all the historical series capacitor SSO events occurred under the radial connection between type-3 WPP and series capacitors, electromagnetic transient (EMT) studies in [35] indicate that SSO could also be triggered under the non-radial connection.

The type-3 wind generation is more vulnerable to series capacitor SSO because IGE could be exacerbated by the inverter control. The industry terms such interaction as subsynchronous control interactions (SSCI) [17] or subsynchronous interaction (SSI) [33]. According to the EMT simulation study results in [17], increasing DFIG rotor side converter current control gain can worsen oscillations.

1) Mitigations: A popular mitigation principle for LC resonant mode is to add damping at the LC resonant frequency range. This can be achieved by designing a virtual resistance to provide damping at SSO frequency while consuming insignificant power at the nominal frequency. This can be achieved in several ways, including design of generator special control, adding resonance damping equipment at the wind farms or the series capacitors, as pointed out by E.V. Larsen [33]. A few examples are listed below.

The first method is to introduce supplementary control loops in the wind turbine's converter controllers so that they have positive damping in the subsynchronous frequency range.

For example, a high-pass filter and potential derivative controller-based mitigation technique has been implemented in four type-3 wind turbines in north China [36]. However, it can sometimes be challenging to add supplementary control loops due to grid code compliance issues or additional labor costs involved in upgrading already commissioned infrastructure.

Non-virtual resistance control methods include employing feedback control loop to modulate the WPP terminal voltage magnitude to counter the series capacitor voltage magnitude [31].

The second potential mitigation solution is to add a specially designed shunt converter-based damping device at the point of connection, e.g., the one proposed in [37]. The shunt converter-based supplementary controller injects subsynchronous currents into the grid and behaves like a virtual resistor at the subsynchronous frequencies. A 10-MVA shunt converter-based SSO damping controller has already been commissioned in the Guyuan WPP in North China. Usually, the damping controller is tuned to operate at a certain oscillation frequency, which is known after frequency scan or post-event analysis. Some algorithms can be adapted to detect and estimate the frequency of the oscillation mode [38].

III. Weak Grid SSO

Events #3-#7, #9-#12, #14-# 19 (total 15 events) are all associated with weak grid operation. For all of these events with the exception of #8 (West China 30-Hz event) and #9 (Hydro One 20-Hz event), oscillations occurred at the conditions when the power level is high and/or the system strength is weak.

Event #8 is exceptional because the oscillation frequency is relatively high for a weak grid event (30 Hz versus a typical 3-10 Hz weak grid oscillations in WPPs) and the oscillation is unaffected by the generation dispatch, even appearing when the WPP was exporting just 5 MW.

Event #9 is exceptional because the oscillation is worse when solar PV power output is low.

A. (2015) West China 30-Hz oscillation event

On July 1st, 2015, type-4 WPPs located in West China experienced oscillations. The wind power is collected at substations A, B and C then transmitted to substation D through 109-km and 134-km long transmission lines. The collected power is then fed to the main 750-kV grid through a 220-kV double circuit transmission line. Station H connects with thermal power plants M (four 660-MW units) and N (two 660-MW units) and connects a ±800 kV HVdc link to transfer the surplus power to the Central China Power Grid. The system topology is shown in Fig. 9. The huge amount of WPPs and the long distances make the short circuit ratio very small; thus, the interconnection is considered weak.
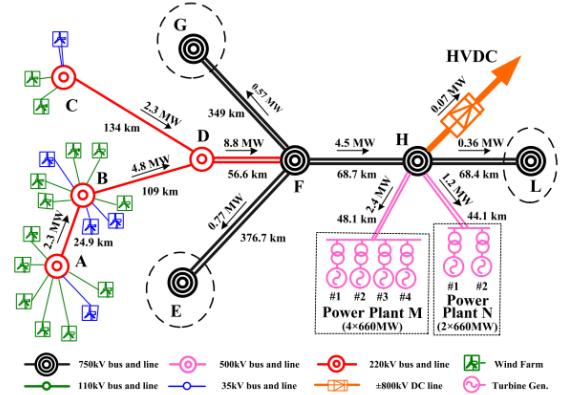

Fig. 9: West China system topology [20]. Source: X. Xie; used with permission.
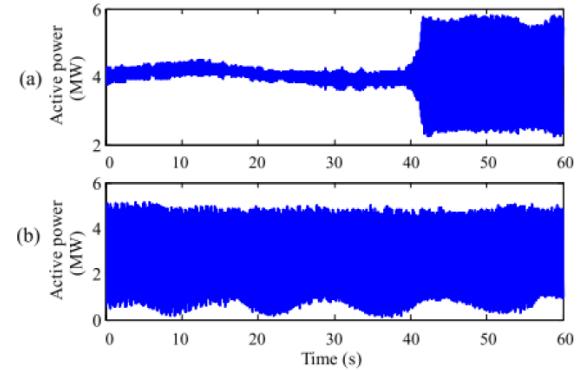
Fig. 10: 2015 West China 30-Hz oscillation event [20]. Source: X. Xie; used with permission.

The oscillations spread across the grid. The oscillation frequency coincided with the torsional frequencies of the thermal power plant M, triggering severe torsional interactions. Eventually, torsional relays tripped the turbo-generators and the power transfer from the HVdc link dropped from 4500 MW to 3000 MW. The field recorded active powers are shown in Fig. 10.

1) Mechanism: Phase-locked loop (PLL) and Torsional Interaction: The west China case shows 30-Hz oscillations appear at an output level of 5% of WPP capacity in a weak grid. The oscillations were speculated to be associated with poor PLL implementation [39]. References [40], [41] confirmed that a PLL with inappropriate parameters can lead to higher frequency SSO. [41] also presents EMT simulation case studies to demonstrate that a weak grid mode caused by a type-4 WPP's PLL can interact with a thermal generator's torsional mode.

B. (2011) Texas 4-Hz oscillations in a WPP

4-Hz oscillations were captured by PMUs (with a sampling rate at 30 Hz) installed at a type-4 WPP in Texas [18].

(a) Poorly-damped oscillation at low output


(b) Un-damped oscillations at high output
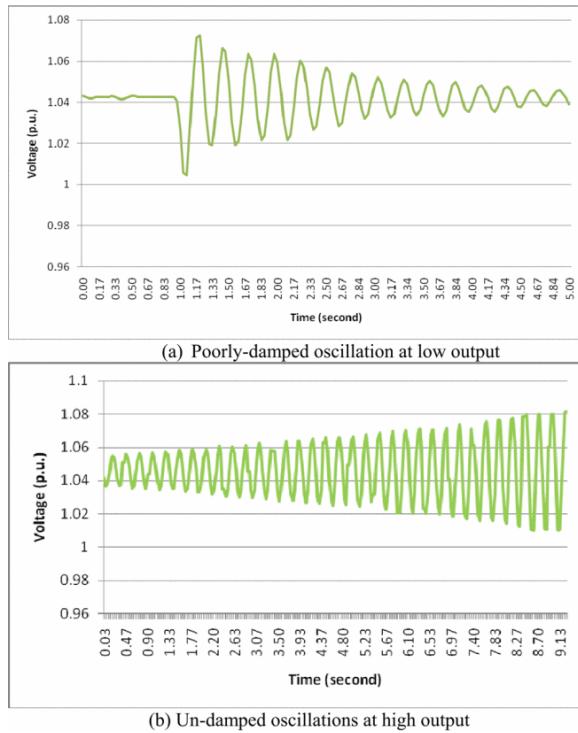
Fig. 11: Texas 4-Hz weak grid oscillations: recorded voltage measurement at a WPP's point of interconnection [18]. Source: ERCOT; used with permission.

At normal conditions, the WPP is connected to the ERCOT grid through one 69-kV transmission line and one 138-kV transmission line. When the 138-kV transmission line was out of service for maintenance, the SCR reduced below 2 and undamped oscillations appeared. Measurement recordings are presented in Fig. 11. ERCOT successfully replicated the oscillation events in the study. The oscillations was identified to be associated with the WPP's voltage control. Slowing down the voltage control can help mitigate the oscillations [18].

C. (2015) Hydro One 20-Hz oscillations in solar PVs

Hydro One observed 20-Hz poorly damped oscillations in RMS voltage measurements at a 44-kV distribution feeder upon switching in a 30-Mvar capacitor in a substation [21]. Three 10-MVA solar PV plants were connected to the utility substation through a 30-km feeder. Fault level at the 44-kV point of connection (PoC) is approximately 120 MVA.

Hydro One also observed that the instantaneous currents and voltage have a large 80-Hz oscillation component. This component reflects in the RMS voltage as 20-Hz oscillations. Fig. 12 presents the recorded instantaneous current and the voltage measurement. The oscillation issue was resolved by closing a tie breaker to reduce grid impedance.

D. (2017) First Solar 7-Hz oscillations

First Solar reported an oscillation event at a 500-MW solar PV farm [24]. The actual measurement data at the PoC,
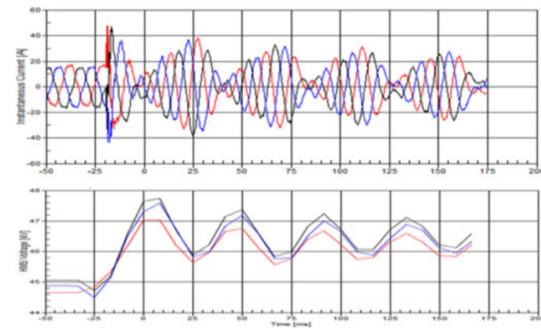

Fig. 12: Hydro One solar PV oscillations [21]. (a) 80-Hz oscillations in the phase current. (b) 20-Hz oscillations in the RMS voltage measurements. Source: C. Li; used with permission.

including real and reactive power output and bus voltage, are shown in Fig. 13. The observed oscillations were attributed to a weak grid condition resulting from a contingency.
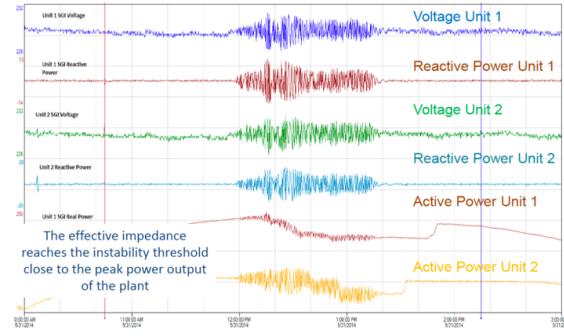

Fig. 13: First Solar 7-Hz oscillations [22]. Source: First Solar; used with permission.

E. (2019) 9-Hz oscillation event in an offshore WPP in GB

During the August 2019 GB power disruption event, an off-shore 799 MW WPP consisting of 7-MW type-4 wind turbines experienced poorly damped 9 Hz oscillations. Ten minutes later, a lightning strike caused a transmission line to trip. The system strength as viewed from the WPP became lower. Undamped oscillations caused the WPP to deload to 60 MW.

An investigation determined that the control system was not tuned properly. This was corrected with a manufacturer control upgrade. Investigation also indicates the cause of poorly damped oscillation was due to WPP's voltage control, an issue similar to the 4-Hz oscillations in Texas.

F. Australia 7-Hz oscillations

In Australia, AEMO observed 7-Hz oscillations in IBR dominated West Murray area as shown in Fig. 14. The west-Murray area is an IBR rich area that host wind farms, solar farms, batteries, HVdc interconnection and static var compensators (SVCs). The 7-Hz oscillations are involved with multiple IBRs. In this region, IBR penetration is very high and the system strength is very low. A similar 7-Hz voltage

oscillations were initially observed in 2015 with 5% peak to peak oscillations.

AEMO conducted simulation studies using wide-area PSCAD modeling which includes original equipment manufacturer (OEM) models of IBRs. Through detailed simulations, it was identified that the magnitude of oscillations can be reduced by lowering the number of online inverters. Further simulation tests show that IBRs have different responses towards the 7-Hz oscillations. Some contribute reactive power in phase with the voltage, some contribute reactive power out of phase with the voltage. Also, some have a major impact while others have a minor impact.
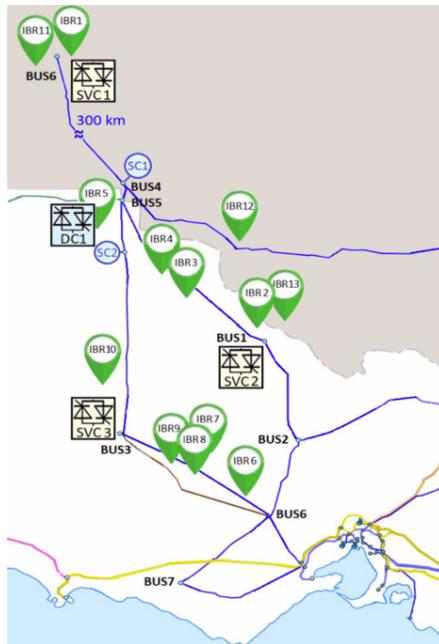

Fig. 14: West Murray region. Source: AEMO; used with permission.
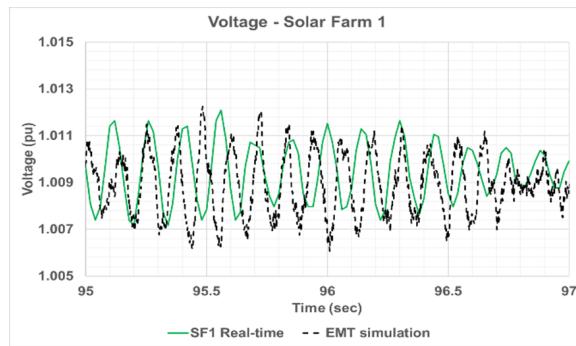
Fig. 15: AEMO 7-Hz oscillations. Voltage after a disturbance. Source: AEMO; used with permission.

In 2019, AEMO carried out system tests to validate the outcome of EMT modelling. Fig. 15 shows the real-time responses compared against EMT simulation.

For mitigation via IBR control system parameter tuning, inverter-level control upgrade has been conducted by the OEM. The upgrade includes PLL parameter and introduction of a fast reactive current compensation loop [26].

G. AEMO 19-Hz oscillations

On 20 August 2020, a transmission fault resulted in a trip of a 220-kV transmission line in northwest Victoria, Australia. This resulted in several wind farms inter-tripped due to a designed runback scheme. After the line and wind/solar farm trip, AEMO has observed 19-Hz voltage oscillations.

The oscillation is highest at the location where the solar farm was tripped, with peak-peak oscillation at around 1% (0.01pu on voltage). These oscillations occurred in both real and reactive power flow from a number of IBRs connected in that area with the magnitude of oscillations ranging from as low as 0.1% to as high as 2%. Fig. 16 shows measured responses.
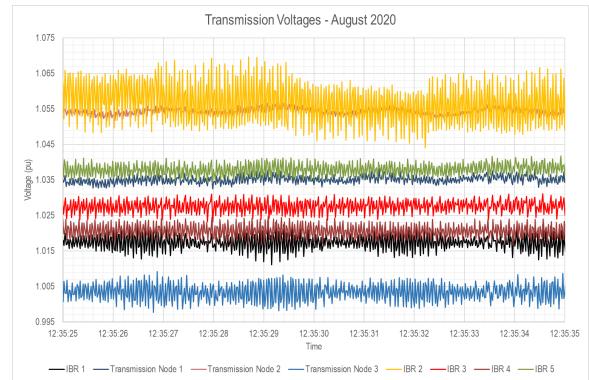
Fig. 16: AEMO 19-Hz oscillations - West Murray area. Source: AEMO; used with permission.

H. Dominion Energy 22-Hz oscillations

An oscillation mode, reported by Dominion Energy, was identified in synchrophasor data measured at solar source penetrated substations with ambient operating conditions [29]. The oscillation mode frequency was found to be 8 Hz from synchrophasor data with 30 frame/second sampling rate. The emergence of this oscillation coincides with the daylight hours as shown by the spectrogram in Fig. 17.
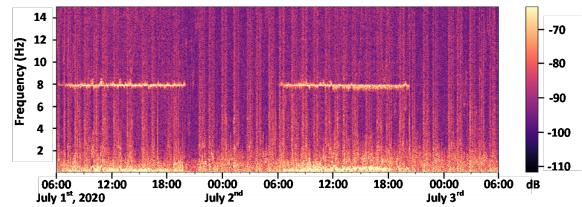
Fig. 17: Dominion Energy 22-Hz oscillations: spectrogram. Source: C. Wang; used with permission.

With further investigations using higher sampling rate data including 60 frames/second synchrophasor data and Point-on-Wave (PoW) data sampled at 960 Hz, it was identified that the frequency of this oscillation is 22 Hz from which the aforementioned 8 Hz mode is aliasing. Power Spectral Density (PSD) plots on PoW data of both voltage and current measurements are shown in Fig. 18 to further validate this finding by showing high energy at 38 Hz (60 Hz – 22 Hz) and 82 Hz (60 Hz + 22 Hz). It can be seen that the energy of

this mode in current measurement is weaker than in voltage which coincides with spectrogram observations.

This phenomenon has been observed in measurements from multiple areas in the system with or without immediate solar penetration. However, it is worth noting that although the oscillation seems significant in frequency domain, the actual magnitude of the oscillation in time domain is minor and it is not affecting normal operation of the grid given the current comparatively limited capacity of the solar sources in the system.
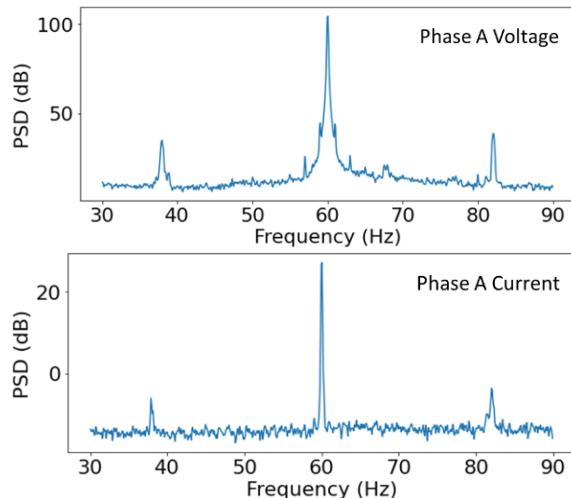
Fig. 18: PSD plots of voltage and current PoW data. Source: C. Wang; used with permission.

IV. Weak Grid SSO Mechanisms: Literature Review

For WPPs in weak grids, oscillations are typically less than 10 Hz, e.g., 4 Hz (#4 Texas), 5 Hz (#5 BPA), 3 Hz (#6 OG&E, #15 Hydro One), 9 Hz (#16 GB), 8 Hz (#19 Scotland). Occasionally, 13-14 Hz oscillations have been reported by BPA (#5), OG&E (#3), and China (#11). For solar PVs, 7-Hz (#12 First solar, #14 AEMO), 17-19 Hz (# 17 AEMO), and 22-Hz (#18 Dominion Energy) oscillations have been reported.

Based on the operation records and event analysis, several possible causes may be associated with weak grid SSO. For example, PLL is associated with the West China 30-Hz event (#8), 7-Hz AEMO event (#14); while voltage control has something to do with the Texas 4-Hz oscillations (#4), the BPA oscillation events (#5), the GB 9-Hz oscillation event (#16).

Mechanism analysis of various weak grid oscillations of a grid-following inverter is an ongoing research topic. In this section, possible causes of oscillations identified by the literature are reviewed.

A. PLL and oscillations

From the power system side, researchers working on HVdc systems have noticed weak grid stability issues of HVdc inverters. For example, back in 1999, Jovcic has shown there is a limitation to transfer power from the inverter to the ac grid and PLL parameters influence stability [42]. In 2010, Strachan and Jovcic published an article on analytical model building of a grid-connected 2 MW type-4 wind turbine [43]. 10-Hz oscillations appear when the grid impedance increases. Eigenvalue and participation factor analysis shows that this mode is influenced by the ac voltage control of the wind turbine grid-connected inverter.

The model in [43] includes not only grid-side converter control detail, but also machine side converter control and type-4 generator dynamics. This results in a high-order (47) state-space model, which poses difficulty for analysis. The SCR discussed in [43] is in the range of 4-10. In the research conducted by Zhou et al. [11], a VSC-HVdc inverter was represented by a 16th-order small signal model. Eigenvalue analysis showed that the weak grid oscillation mode was greatly influenced by the PLL parameters. Furthermore, it demonstrated, by using a lower PLL gain, the converter can operate in a very weak system with an SCR of 1.3.

The research in [11] implicates two important findings: (i) the gains of the PLL, particularly for weak grids, greatly affect the operation of the VSC-HVdc converter; (ii) for very weak grid (e.g., SCR at 1.3), PLL with high gains may pose instability issue. The work in [11] opened the path of eigenvalue analysis with EMT-level detail models for VSC dynamics, which later inspired many follow up research, e.g., [40], [41].

From the power electronics community, impact of PLL on stability has been examined for frequency-domain responses using impedance/admittance models. In both [44] and [45], Harnefors et al. derived a VSC's admittance model with current control, PLL and outer dc-link voltage control included. It is found that PLL with a high bandwidth and dc-link voltage control with a high bandwidth may introduce instability. This finding on PLL is also echoed by another group of researchers [46]. [46] finds that PLL introduces negative incremental resistance in the qq-component of the VSC impedance. Under weak grid conditions, increasing PLL's bandwidth may lead to instability.

We may fast forward to a recent article in IEEE trans. Power Systems [47] on weak grid oscillations. This paper summarizes the remarks of the past literature and indicates that oscillations can occur due to (i) PLL of high-frequency bandwidth only, (ii) interaction of PLL of high-frequency bandwidth with inner current control, and (iii) interaction of PLL of low-frequency bandwidth with outer control. The third cause may lead to low-frequency SSOs (typically less than 10 Hz). This cause has also been presented in [48] with a detailed block-diagram based analysis to demonstrate that the interaction of dc-link control and PLL can lead to SSOs. Though [47] employed linear model only for analysis and demonstration, the remarks can serve as a reference.

B. Outer control mode and low-frequency SSOs

Since [47] is based on a grid-following converter control regulating the dc-link voltage and reactive power, other possible causes of low-frequency SSOs, e.g., voltage control, have not been mentioned. Indeed, outer control mode matters whether low-frequency SSOs may appear or not.
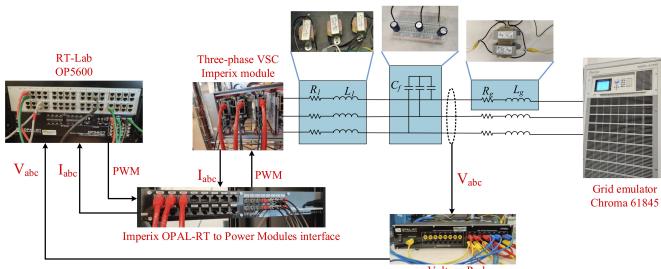
Fig. 19: Configuration of the hardware test bed at University of South Florida [49].

From the power grid operation view, weak grid instability can be viewed as dynamic voltage stability issue. Pushing more power into a weak grid will cause voltage reduction. The reduction of voltage will cause less power to be delivered. This characteristic, similar to voltage instability, introduces an unstable feedback loop, as discovered in [50]. In turn, [51] has shown that faster ac voltage control or introducing a feedback loop to decouple voltage and power can improve weak grid stability.

Yet, whether the system will suffer low-frequency SSOs or not may depend on outer control mode and outer power control parameters, if the PLL has a low-frequency bandwidth and the inner current control is very fast.

Both EMT simulation and hardware experiments have been conducted by the task force members at University of South Florida [49] to demonstrate weak grid oscillations or weak grid voltage instability without oscillations. The inverter control is assumed to be in PQ following mode or PV control mode.

Fig. 19 presents the hardware test bed configuration and Fig. 20 presents the experiment results. It can be seen that if the power control is slow, PQ control leads no oscillation while PV control leads to 3-Hz oscillations. If the power control is tuned to be fast, even in PQ control mode, 3-Hz oscillations appear.

V. COMPARISON AND DEEP THINK

By reviewing the literature, comparing the field record data of the listed events, five questions may be posed.

- In the literature, grid-following inverter with fast voltage control is claimed to improve stability [51]. On the other hand, ERCOT experience shows that slowing voltage control can mitigate 4-Hz oscillations [18]. Why the literature and the field experience give two different answers?
- Are there connections between series LC resonance mode and overcurrent?
- Can the phase voltage/current spectrum give us clue on causations?
- Type-3 WPPs connected to series compensated lines have shown to be vulnerable to SSO. Will there be potential risks of SSO for type-4 wind farms and solar PVs when connected to series compensated lines?
- Shunt compensation has been widely used in wind farms and solar PVs. Will there be potential risks of SSO due to shunt compensation and IBR interactions?

A. Deep Think 1: Is fast voltage control good or bad for low-frequency SSOs?

The key difference between [51] and the ERCOT case is that [51] refers to the inverter-level voltage control where communication and control delay is negligible, while in the ERCOT case, the voltage control refers to the plant-level control where delay cannot be ignored. Majority of the research papers have not considered plant-level control. Hence, Texas 4-Hz oscillations have not been adequately explained. In this article, we attempt to offer a reasonable explanation on why fast voltage control is bad in this case.

A very simple block diagram is constructed to illustrate the voltage control closed-loop system and the effect of delay on such system. At the plant level, the voltage regulator amplifies the voltage error and generates a reactive power command. The communication delay is T_d to send this command to the inverter. Considering the plant-level control to inverter-level communication delay, a time delay of 0.1 s may be assumed.

It is well known that the PCC voltage and the injected reactive power relationship can be represented as $\Delta V = X_g \Delta Q$. In addition, we may consider a first-order lagging unit to represent the reactive power following control:

$$\frac{\Delta Q}{\Delta Q^{\text{ref}}} = \frac{1}{1 + \tau s}.$$

Thus, the entire closed-loop system can be drawn as Fig. 21. With the delay unit represented by a first-order Pade approximation, the root loci of the open-loop system ($OL(s)$) is shown in Fig. 22 for two types of voltage regulator: integral control or PI control.

The expression of $OL(s)$ is as follows:

$$OL(s) = \frac{K_i}{s} \frac{1 - 0.05s}{1 + 0.05s} \underbrace{\frac{X_g}{1 + \tau s}}_{G_{QV}}. \tag{1}$$

It can be seen that the communication delay introduces a zero in the right-half-plane (RHP), which attracts two root loci. Oscillations at 2 Hz may appear if the open-loop gain is increased to 2.63. Increasing X_g or K_i can make the system unstable with oscillations. If the PI voltage controller is used, the system approaches instability at a gain of 2.91 and 4.6-Hz oscillations may appear.

Remark: Increasing plant-level voltage control gain can make low-frequency SSOs worse. A key factor to be considered is the communication delay of plant-level control. 100 ms delay largely is the main contributor of the low-frequency SSOs.

While the above model can explain why reducing voltage control gain can mitigate oscillation, it does not have the capability to explain why oscillations are undamped during high power scenarios while oscillations are well damped during low power exporting scenarios. This model only considers the reactive power's effect on voltage. On the other hand, in weak grid condition, real power also has a significant impact on the point of common coupling (PCC) voltage. It is well known from steady-state voltage stability point of view that exporting more real power may lead to decrease in voltage. Interested
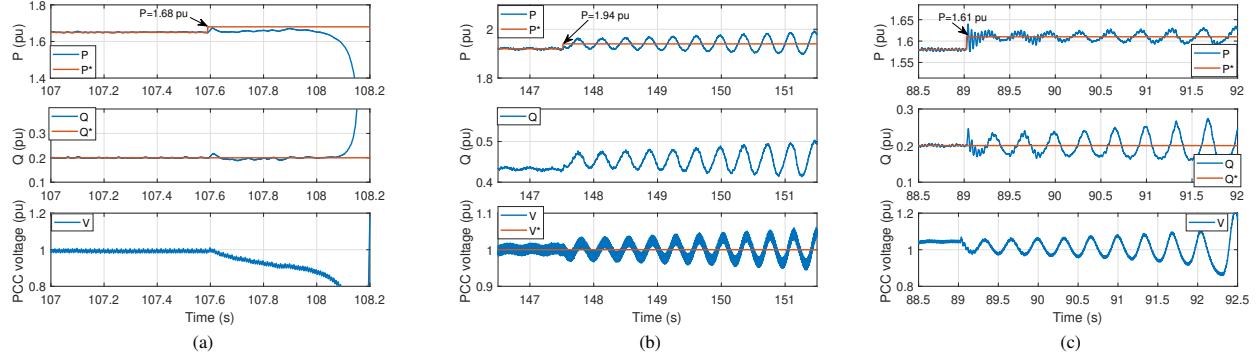
Fig. 20: Hardware experiment results [49] (The responses of P, Q and voltage when P is given a step change) demonstrating weak grid instability. (a) PQ control mode (slow P control): losing stability without subject to oscillations. (b) PV control mode (slow P control): oscillations. (c) PQ control (fast P control): oscillations appear when the power control becomes fast.
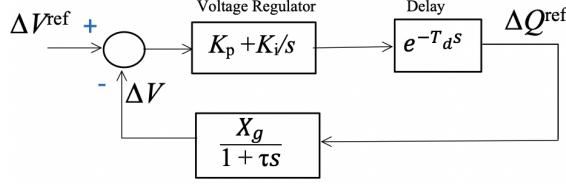

Fig. 21: Voltage control closed-loop system. $K_p = 0$ or 1, $K_i = 10$, $T_d = 0.1$ s, $\tau = 0.04$, $X_g = 0.5$.
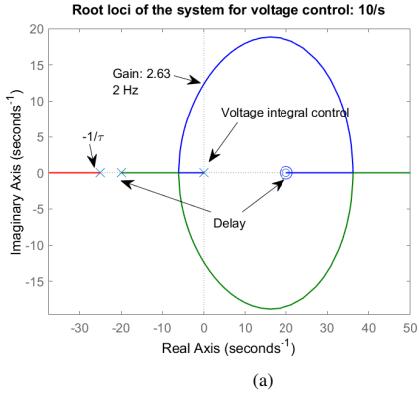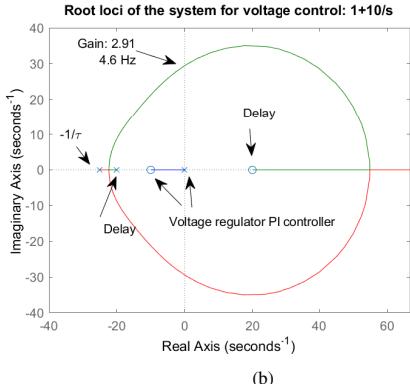
Fig. 22: The root loci of the open-loop system. Voltage control: (a) integral control. (b) PI control.

readers may refer to [50], [51] for more information on power exporting level's effect on stability.

In summary, the effect of plant-level control is recommended to be included for further comprehensive investigation.

B. Deep Think 2: Series LC mode and overcurrent

The Minnesota, Texas, and North China events are all due to type-3 wind farms radially connected to series compensated transmission lines. In all these events, three-phase instantaneous currents demonstrate large overcurrent. It can be easily understood that overcurrent is due to the small electric network impedance at the LC resonant frequency. Spectrum of phase current also shows one dominant subsynchronous components besides the fundamental component. For example, for the Texas series capacitor SSO, Fig. 5 shows a dominant 26 Hz component.

On the other hand, if we examine the Hydro One event, we also see overcurrent at 80 Hz. Co-author C. Li also conducted spectrum analysis for phase current and the dominant component is 80 Hz. This gives us a hint to examine if there is indeed a series LC mode at 80 Hz.

The electric network has only shunt compensation and the LC modes are at a frequency over 200 Hz. Therefore, it is reasonable to ask this question: Is it possible that the solar PV act as a voltage source behind a series capacitor at 80-Hz frequency region? Is it possible that this feature causes a dip in the total impedance magnitude, which makes overcurrent possible? The NERC event report of the 2020 San Fernando large-scale solar tripping event [3] shows that slow converter current control leads to overcurrent. A quantitative analysis [52] indeed shows that slow inverter current control introduces a dip in the total impedance magnitude, which in turn results in overcurrent.

A numerical case can be constructed based on the feeder data provided in [21] and the assumed solar PV inverter control structure and parameters. Fig. 23 presents the test system circuit topology and the assumed PV inverter control structure, where the inner current control is implemented in the static frame using proportional resonant (PR) control and the control delay is modeled as $T_d = e^{-\tau s}$.

Consider the inner current control, delay effect only, the impedance of the solar PV Z_{PV} can be found and an unstable 80-Hz mode in the static frame can be created by tuning parameters.

Fig. 24a presents the PV impedance and the grid impedance. It can be seen that the two impedances have the same magnitudes at 80 Hz, which means that the open-loop transfer

12
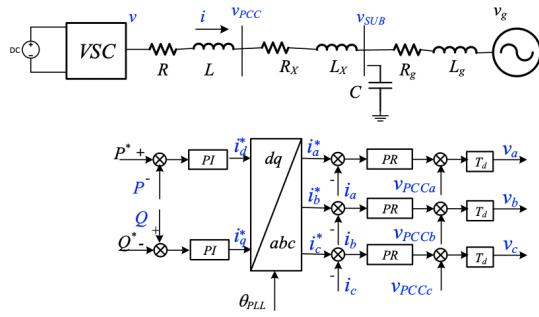
Fig. 23: The circuit topology and assumed inverter control structure for the Hydro One event. The detailed data are provided in Table I.

TABLE I: Per Unit Data of the test bed in Fig. 23.

choke filter	R, L	0.015, 0.15	assumed
Feeder to the substation	R_x, L_x	0.0651, 0.1805	grid data
Source impedance	R_g, L_g	0.007, 0.0698	grid data
Shunt capacitor	C	1	grid data
Inverter current control	PR	$0.02 + 2\frac{2\omega_c s}{s^2+2\omega_c s+\omega^2}$	assumed
Control delay	τ	200 μs	assumed

$\omega_c = 2\pi \times 2$ rad/s and ω is 377 rad/s.

(a)

(b)

Fig. 24: (a) The PV impedance and the grid impedance. Crossover frequency is 80 Hz. Phase difference between the two impedances are greater than 180 degree, implicating instability. (b) The total impedance shows a dip at 80 Hz.

function $Z_{\mathrm{PV}}/Z_{\mathrm{grid}}$ has a crossover frequency at 80 Hz. The phase difference between the two impedances are over 180 degree, implicating an unstable 80-Hz oscillation mode. Fig. 24a(b) shows that the total impedance has a dip at 80 Hz.

Furthermore, Fig. 24a also presents the grid impedance when the shunt capacitor is not connected. The shunt capacitor introduces a peak in the grid impedance magnitude at 229 Hz and a dip at 269 Hz. It can be seen that the shunt capacitor only influences the magnitude and phase angle of the grid impedance at the frequency range above 200 Hz. For the frequency range below 100 Hz, the shunt capacitor does not influence the grid impedance.

Thus, it can be concluded that the shunt capacitor does not contribute to the oscillation mode. Rather, energizing the shunt capacitor triggers the 80-Hz oscillation mode.

So far, for this event, we still haven't explained why oscillations are more severe during low power output conditions. A more comprehensive analysis has been conducted in a recently submitted paper. Interested readers may refer to [53].

C. Deep Think 3: Phase current spectrum signature

In all these series capacitor SSO events, spectrum of the three-phase instantaneous currents shows one dominant subsynchronous component besides the fundamental component.

This is not the case for many other events.

In the case of Event #11, both 37-Hz and 63-Hz oscillations were observed in the phase voltage and currents of a type-3 WPP with weak grid interconnection. Fig. 25 presents the frequency spectrum of the phase voltage and phase current measured at a STATCOM installed at the WPP. The two components are symmetrical in the current spectrum. In the voltage spectrum, the 63-Hz component is more dominant.

Event #18 is associated with solar PVs and 22-Hz oscillations were observed in RMS measurements. In phase
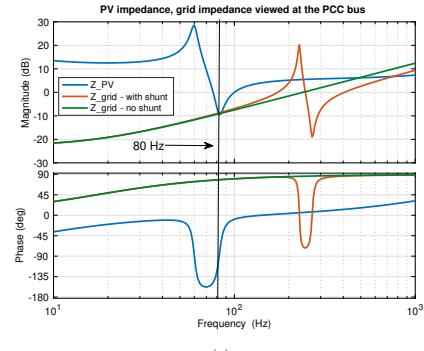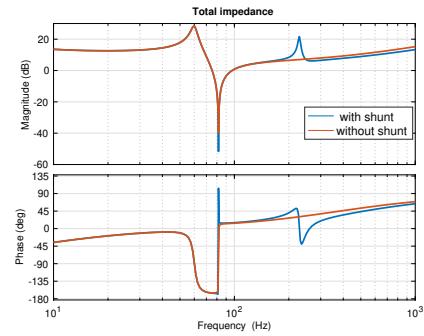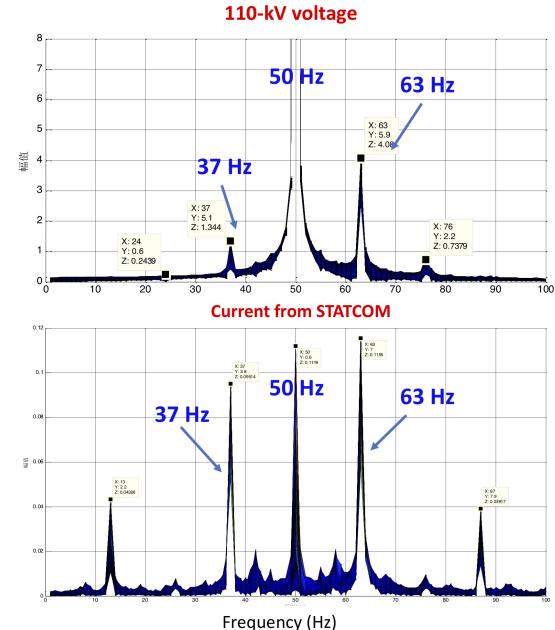

Fig. 25: The spectrum data of phase voltage and current of Event #11 show both 37-Hz and 63-Hz oscillation components. Source: X. Xie.

voltage and current, both 38-Hz and 82-Hz components have comparable magnitudes.

Indeed, the current and voltage spectrums (Fig. 8) in [45] for PLL introduced oscillations have a quite similar feature as Event #11. Thus, it is reasonable to speculate this event may be associated with PLL.

Furthermore, it is reasonable to speculate the following:

different causation leads to different signatures in phase current spectrum, especially on those mirrored frequency components. Such signatures cannot be detected if only RMS measurements are collected or if only RMS-based simulation is conducted. The difference in phase spectrum also motivates further research to understand why. A straightforward and rough explanation can be that if the oscillations are originated from the electric network, one mode will be predominant. On the other hand, if the oscillations are due to dq-frame control which leads to modulation on angle, voltage magnitude or current magnitude, the resulting spectrum of phase current and voltage may show two comparable components of mirrored frequencies.

Refined analysis and EMT-model based simulation are required to understand the connection between phase variable spectrum and oscillation causation. This also motivates this task force to construct EMT test beds and examine phase variable spectrums for oscillations of different mechanism in [53].

D. Deep Think 4: Interaction of series compensation and grid-connected converters

Both type-4 wind farms and solar PVs employ grid-following converter control. Thus, the question can be viewed as if there are potential interactions of the electric LC resonance mode with converter controls.

The task force members at University of South Florida has carried out a study to examine a scenario of type-4 WPP radially connected to a series compensated line [54]. It is found that it is possible to see interaction of PLL and the LC mode. This interaction may lead to SSO. If PLL has a low bandwidth, increasing series compensation reduces grid impedance and leads to better stability. On the other hand, if PLL has a high bandwidth, increasing series compensation may lead to worse SSO by pushing the mode of PLL to the right-half-plane.

Further comprehensive analysis is needed to identify interactions of series compensation and VSC controls.

E. Deep Think 5: Interaction of shunt compensation and grid-connected converters

Similarly, it is valid to examine if there are potential interactions of shunt compensation and converter controls, e.g., PLL.

Shunt compensation is popularly employed in WPPs and solar PVs. When the grid is strong, the LC mode has a high frequency. The Hydro One case shows that when the SCR is 4 and the shunt compensation is 1 p.u., the LC mode has a frequency over 200 Hz. If the SCR is reduced to 1.8, the frequency of the LC mode will be reduced to 80 Hz. Such a mode viewed in the dq frame will have a frequency of 20 Hz when SCR is 1.8 and 140 Hz when SCR is 4. In the first case, it is very possible that this mode may interact with PLL and cause SSO in dq frame. In the second case, it is also possible that this mode may interact with current control.

In summary, an examination of the events leads to many in-depth thinking. We pose the above five questions and the task force will continue to work to address the questions by carrying out more in-depth investigations.

VI. CONCLUSIONS AND CHALLENGES

In this paper, we have documented a list of IBR SSOs. The first type is associated with the interaction of type-3 WPPs and series capacitors. This type is termed *series capacitor SSO*. The second type is associated with weak grids and it is termed *weak grid SSO*. This work of documenting, review, and comparison of real-world IBR SSO events is of uttermost importance to develop a better understanding of IBR related dynamics, as an event may present a unique feature that has not been captured before.

We would like to point out one single example to show how real-world operating experience and data can help shape research to be rigorous and thorough. While majority weak grid SSOs become worse with increased power transfer level, there is one exception: the Hydro One event. In that case, oscillations were obvious in the morning when solar PV power output is light. With many papers published on IBR weak grid oscillation stability, are there any research papers that capture this subtle yet important detail? To the authors' best knowledge, the answer is No.

Thus, we can clearly see, with all the initial research, the work of developing a fundamental understanding and mitigation strategies for various types of SSOs just begins and is expected to remain a challenge with higher and higher IBR penetration and new types of control (e.g., grid forming control) introduced. Rigorous and thorough research as well as cross validation from industry operation are imperative to achieve the goal.

A challenge facing the grid industry and the academic community is the lack of IBR models. As stated by E.V. Larsen [33], strict nondisclosure requirements are imposed by vendors. Such fact makes modeling of IBR an intellectual challenge. We need not only prior knowledge of power electronic converter control but also field measurements to develop models and refine models. Close collaboration between researchers and operation industry is important to develop relevant research to the practical world.

Last but not least, advanced measurement devices are necessary. For IBR SSOs, not only RMS measurements but also three-phase measurements are necessary to better understand each phenomenon. To this end, advanced sensing technology with high data resolutions, such as PoW adopted by Dominion Energy, becomes indispensable.

REFERENCES

[1] J. Matevosyan, "Survey of grid-forming inverter applications," G-PST/ESIG webinar, June 10, 2021. [Online]. Available: http://w3techs.com/technologies/overview/content_language/all

[2] Joint NERC and WECC Staff., "(2018, February) 900 MW Fault Induced Solar Photovoltaic Resource Interruption Disturbance Report: Southern California Event: October 9, 2017."

[3] Joint NERC and WECC Staff Report, "(2020, November) San Fernando Disturbance, South California Event: July 7, 2020."

[4] (2017, September) Reliability Guideline Forced Oscillation Monitoring & Mitigation. NERC.

[5] IEEE PES WindSSO Taskforce, "PES TR-80: Wind Energy Systems Subsynchronous Oscillations: Events and Modeling, 2020," https://resourcecenter.ieee-pes.org/publications/technical-reports/PES_TP_TR80_AMPS_WSSO_070920.html.

[6] N. Hatziargyriou, J. Milanovic, C. Rahmann, V. Ajjarapu, C. Canizares, I. Erlich, D. Hill, I. Hiskens, I. Kamwa, B. Pal et al., "Definition and classification of power system stability revisited & extended," IEEE Transactions on Power Systems, 2020.

[7] B. Badrzadeh, Z. Emin, S. Goyal, S. Grogan, A. Haddadi, A. Halley, A. Louis, T. Lund, J. Matevosyan, T. Morton, D. Premm, and S. Sproul, "System strength," CIGRE Science and Technology Journal, vol. 21, February 2021.

[8] AEMO, "System strength workshop," accessed: June 19, 2021. [Online]. Available: https://aemo.com.au/en/learn/energy-explained/system-strength-workshop.

[9] Subsynchronous Resonance Working Group of the System Dynamic Performance Subcommittee, "Reader's guide to subsynchronous resonance," IEEE Transactions on Power Systems, vol. 7, no. 1, pp. 150–157, 1992.

[10] "Torsional interaction between electrical network phenomena and turbine-generator shafts: Plant vulnerability," ERPI Technical report 1013460, 2006.

[11] J. Z. Zhou, H. Ding, S. Fan, Y. Zhang, and A. M. Gole, "Impact of short-circuit ratio and phase-locked-loop parameters on the small-signal behavior of a vsc-hvdc converter," IEEE Transactions on Power Delivery, vol. 29, no. 5, pp. 2287–2296, 2014.

[12] M. Parniani and M. Iravani, "Voltage control stability and dynamic interaction phenomena of static var compensators," IEEE transactions on power systems, vol. 10, no. 3, pp. 1592–1597, 1995.

[13] C. Buchhagen, C. Rauscher, A. Menze, and J. Jung, "Borwin1-first experiences with harmonic interactions in converter dominated grids," in International ETG Congress 2015; Die Energiewende-Blueprints for the new energy age. VDE, 2015, pp. 1–7.

[14] Ł. H. Kocewiak, J. Hjerrild, and C. L. Bak, "Wind turbine converter control interaction with complex wind farm systems," IET Renewable Power Generation, vol. 7, no. 4, pp. 380–389, 2013.

[15] A. Mulawarman and P. Mysore, "Detection of undamped subsynchronous oscillations of wind generators with series compensated lines," in Minnesota Power Systems Conference, 2011.

[16] P. Belkin, "Event of 10/22/09." [Online]. Available: http://www.ercot.com/content/meetings/rpg-crez/keydocs/2010/0126/8Belkin_Event%20of%2010.ppt,2009

[17] G. D. Irwin, A. K. Jindal, and A. L. Isaacs, "Sub-synchronous control interactions between type 3 wind turbines and series compensated ac transmission systems," in 2011 IEEE Power and Energy Society General Meeting. IEEE, 2011, pp. 1–6.

[18] S.-H. Huang, J. Schmall, J. Conto, J. Adams, Y. Zhang, and C. Carter, "Voltage control challenges on weak grids with high penetration of wind generation: Ercot experience," in 2012 IEEE Power and Energy Society General Meeting. IEEE, 2012, pp. 1–7.

[19] X. Xie, X. Zhang, H. Liu, H. Liu, Y. Li, and C. Zhang, "Characteristic analysis of subsynchronous resonance in practical wind farms connected to series-compensated transmissions," IEEE Transactions on Energy Conversion, vol. 32, no. 3, pp. 1117–1126, 2017.

[20] H. Liu, X. Xie, J. He, T. Xu, Z. Yu, C. Wang, and C. Zhang, "Subsynchronous interaction between direct-drive pmsg based wind farms and weak ac networks," IEEE Transactions on Power Systems, vol. 32, no. 6, pp. 4708–4720, 2017.

[21] C. Li, "Unstable operation of photovoltaic inverter from field experiences," IEEE Transactions on Power Delivery, vol. 33, no. 2, pp. 1013–1015, 2017.

[22] I. Vieto, G. Li, and J. Sun, "Behavior, modeling and damping of a new type of resonance involving type-iii wind turbines," in 2018 IEEE 19th Workshop on Control and Modeling for Power Electronics (COMPEL). IEEE, 2018, pp. 1–8.

[23] J. Sun and I. Vieto, "Development and application of type-iii turbine impedance models including dc bus dynamics," IEEE Open Journal of Power Electronics, vol. 1, pp. 513–528, 2020.

[24] First Solar, "Deploying Utility-Scale PV Power Plants in Weak Grids," 2017 PES General Meeting, Chicago, IL, July 2017.

[25] B. Badrzadeh, N. Modi, N. Crooks, and A. Jalali, "Power system operation with reduced system strength for inverter-connected generation during prior outage conditions," CIGRE SCIENCE & ENGINEERING, vol. 17, pp. 141–149, 2020.

[26] A. Jalali, B. Badrzadeh, J. Lu, N. Modi, and M. Gordon, "System strength challenges and solutions developed for a remote area of australian power system with high penetration of inverter-based resources," CIGRE SCIENCE & ENGINEERING, vol. 20, pp. 27–37, Feb 2021.

[27] C. Li and R. Reinmuller, "Asset condition anomaly detections by using power quality data analytics," in 2019 IEEE Power & Energy Society General Meeting (PESGM). IEEE, 2019, pp. 1–5.

[28] (2020, January) GB power system disruption on 9 August 2019. [Online]. Available: https://assets.publishing.service.gov.uk/government/uploads/system/uploads/attachment_data/file/836626/20191003_E3C_Interim_Report_into_GB_Power_Disruption.pdf

[29] "(2021, April) Identifying Oscillations Injected by Inverter-Based Solar Energy Sources in Dominion Energy's Service Territory using Synchrophasor Data and Point-on-Wave Data." [Online]. Available: https://naspi.org/sites/default/files/2021-04/D1S102wangdominionnaspi20210413.pdf

[30] Julian Leslie. (2022, January) G-PST/ESIG Webinar Series: Managing Grid Stability in a High IBR Network. [Online]. Available: https://www.esig.energy/event/webinar-managing-grid-stability-in-a-high-ibr-network/

[31] Y. Li, L. Fan, and Z. Miao, "Replicating real-world wind farm ssr events," IEEE Transactions on Power Delivery, vol. 35, no. 1, pp. 339–348, 2019.

[32] L. Fan and Z. Miao, "Nyquist-stability-criterion-based ssr explanation for type-3 wind generators," IEEE Transactions on Energy Conversion, vol. 27, no. 3, pp. 807–809, 2012.

[33] E. V. Larsen, "Wind generators and series-compensated ac transmission lines," in PES T&D 2012. IEEE, 2012, pp. 1–4.

[34] Z. Miao, "Impedance-model-based ssr analysis for type 3 wind generator and series-compensated network," IEEE Transactions on Energy Conversion, vol. 27, no. 4, pp. 984–991, 2012.

[35] Y. Cheng, S. H. Huang, and J. Rose, "A series capacitor based frequency scan method for ssr studies," IEEE Transactions on Power Delivery, vol. 34, no. 6, pp. 2135–2144, 2019.

[36] J. Shair, X. Xie, Y. Li, and V. Terzija, "Hardware-in-the-loop and field validation of a rotor-side subsynchronous damping controller for a series compensated dfig system," IEEE Transactions on Power Delivery, vol. 36, no. 2, pp. 698–709, 2020.

[37] X. Zhang, X. Xie, J. Shair, H. Liu, Y. Li, and Y. Li, "A grid-side subsynchronous damping controller to mitigate unstable ssci and its hardware-in-the-loop tests," IEEE Transactions on Sustainable Energy, vol. 11, no. 3, pp. 1548–1558, 2019.

[38] J. Shair, X. Xie, J. Yang, J. Li, and H. Li, "Adaptive damping control of subsynchronous oscillation in dfig-based wind farms connected to series-compensated network," IEEE Transactions on Power Delivery, 2021.

[39] J. Sun, M. Li, Z. Zhang, T. Xu, J. He, H. Wang, and G. Li, "Renewable energy transmission by hvdc across the continent: system challenges and opportunities," CSEE Journal of Power and Energy Systems, vol. 3, no. 4, pp. 353–364, 2017.

[40] L. Fan and Z. Miao, "Wind in weak grids: 4 hz or 30 hz oscillations?" IEEE Transactions on Power Systems, vol. 33, no. 5, pp. 5803–5804, 2018.

[41] Y. Li, L. Fan, and Z. Miao, "Wind in weak grids: Low-frequency oscillations, subsynchronous oscillations, and torsional interactions," IEEE Transactions on Power Systems, vol. 35, no. 1, pp. 109–118, 2019.

[42] D. Jovcic, N. Pahalawaththa, and M. Zavahir, "Analytical modelling of hvdc-hvac systems," IEEE Transactions on Power Delivery, vol. 14, no. 2, pp. 506–511, 1999.

[43] N. P. Strachan and D. Jovcic, "Stability of a variable-speed permanent magnet wind generator with weak ac grids," IEEE Transactions on Power Delivery, vol. 25, no. 4, pp. 2779–2788, 2010.

[44] L. Harnefors, M. Bongiorno, and S. Lundberg, "Input-admittance calculation and shaping for controlled voltage-source converters," IEEE transactions on industrial electronics, vol. 54, no. 6, pp. 3323–3334, 2007.

[45] L. Harnefors, X. Wang, A. G. Yepes, and F. Blaabjerg, "Passivity-based stability assessment of grid-connected vscs—an overview," IEEE

Journal of emerging and selected topics in Power Electronics, vol. 4, no. 1, pp. 116–125, 2016.

[46] B. Wen, D. Boroyevich, R. Burgos, P. Mattavelli, and Z. Shen, "Analysis of d-q small-signal impedance of grid-tied inverters," *IEEE Transactions on Power Electronics*, vol. 31, no. 1, pp. 675–687, 2016.

[47] W. Du, Y. Wang, Y. Wang, H. F. Wang, and X. Xiao, "Analytical examination of oscillatory stability of a grid-connected pmsg wind farm based on the block diagram model," *IEEE Transactions on Power Systems*, vol. 36, no. 6, pp. 5670–5683, 2021.

[48] Y. Huang, X. Yuan, J. Hu, and P. Zhou, "Modeling of vsc connected to weak grid for stability analysis of dc-link voltage control," *IEEE Journal of Emerging and Selected Topics in Power Electronics*, vol. 3, no. 4, pp. 1193–1204, 2015.

[49] L. Bao, L. Fan, Z. Miao, and Z. Wang, "Hardware demonstration of weak grid oscillations in grid-following converters," *the 53rd NAPS*, 2021.

[50] L. Fan and Z. Miao, "An explanation of oscillations due to wind power plants weak grid interconnection," *IEEE Transactions on Sustainable Energy*, vol. 9, no. 1, pp. 488–490, 2018.

[51] Y. Li, L. Fan, and Z. Miao, "Stability control for wind in weak grids," *IEEE Transactions on Sustainable Energy*, vol. 10, no. 4, pp. 2094–2103, 2018.

[52] L. Fan and Z. Miao, "Root cause analysis of ac overcurrent in july 2020 san fernando disturbance," *IEEE Transactions on Power Systems*, vol. 36, no. 5, pp. 4892–4895, 2021.

[53] L. Fan, Z. Miao, S. Shah, Y. Cheng, J. Rose, S.-H. Huang, B. Pal, X. Xie, N. Modi, S. Wang, and S. Zhu, "Real-world 20-hz ibr subsynchronous oscillations: Signatures and mechanism analysis," *submitted, IEEE trans. Energy Conversion*.

[54] Y. Xu, M. Zhang, L. Fan, and Z. Miao, "Small-signal stability analysis of type-4 wind in series-compensated networks," *IEEE Transactions on Energy Conversion*, vol. 35, no. 1, pp. 529–538, 2019.